Prediction of Scattered Fine-Scale Jet Mixing Noise using Lilley's Acoustic Analogy

A. N. Carr and S. A. E. Miller

Department of Mechanical and Aerospace Engineering
University of Florida

AIAA Scitech, 2020
Orlando, Fl

Acknowledgements

- This research was funded by the University of Florida Graduate School Preeminence Award (GSPA).
- My colleagues at the University of Florida Theoretical Fluid Dynamics and Turbulence Group for many helpful discussions.

Outline

Motivation

- Fine-scale jet mixing noise contributes to noise produced around civilian and military airfields.
- Fine-scale noise is present in downstream, upstream and sideline directions.
- Good candidate for studying mean flow refraction effects.
- Shielding techniques to reduce noise pollution must account for propagation of the fine-scale noise.

Objectives

- Model the fine-scale jet mixing noise with an acoustic analogy type approach.
- Capture the refraction effects using a Green's function solution to Lilley's equation.
- Compare to experimental measurements of subsonic jet noise.
- Implement a tailored Green's function to capture shielding effects of a flat plate, compare with experiment.

Literature Review

- Brown and Bridges [1] obtained spectral measurements of a free-jet for a comprehensive range of jet operating conditions.
- Brown [2] studied the effect of a flat plate below a jet at different distances. Found that high-frequency noise was impacted more significantly from shielding effects.
- Khavaran et al. [3] obtained supersonic jet mixing noise predictions using MGB code. CFD computations with $k - \epsilon$ model to simulate jet flow.
- Khalighi et al. [4] performed LES simulations with a Ffowcs-Williams and Hawkings [5] surface to obtain acoustic predictions.

Literature Review

- LES
  - Benefits: unsteady data $\rightarrow$ source correlations.
  - Drawbacks: computational cost.
- Tam and Auriault [6] predict the fine-scale mixing noise by solving the linearized Euler equations.
  - Source term: kinetic theory based argument $q_s = \frac{2}{3}\rho k_s$.
  - Green's function: adjoint numerical solution.
- Morris and Farassat [7] compared the work of Tam and Auriault [6] to Lighthill's acoustic analogy. Found that when the source term is consistent, the predictions in the sideline direction are similar.

Present Approach

- Lilley's acoustic analogy approach to model the fine-scale mixing noise and refraction effects of the jet shear layer.
  - Step 1: Rearrange the linearized Euler equations to obtain Lilley's equation.
  - Step 2: Manipulate the solution integral to recover the source term of Tam and Auriault [6].
  - Step 3: Derive spectral density integral.
  - Step 4: Implement an appropriate Green's function solution to Lilley's equation and obtain spectral predictions.
  - Step 5: Incorporate shielding effects by tailoring Green's function.

Linearized Euler Equations

- Start with the Favre-averaged Navier-Stokes equation,

$$\bar{\rho}\frac{D\tilde{u}_i}{Dt} = \frac{\partial}{\partial x_j}\left(-\bar{p}\delta_{ij} + \bar{\tau}_{ij} - \overline{\rho u_i' u_j'}\right). \tag{1}$$

- Approximating the Reynolds stresses by Boussinesq [8] eddy viscosity model and closing with the linearized equation of energy,

$$\bar{\rho}\left[\frac{\partial u_i}{\partial t} + \bar{u}_j\frac{\partial u_i}{\partial x_j} + u_j\frac{\partial \bar{u}_i}{\partial x_j}\right] + \frac{\partial p}{\partial x_i} = -\frac{\partial q_s}{\partial x_i} \tag{2}$$

$$\frac{\partial p}{\partial t} + \bar{u}_j\frac{\partial p}{\partial x_j} + \gamma\bar{p}\frac{\partial u_j}{\partial x_j} = 0. \tag{3}$$

- Equations 2 and 3 can be rearranged to Lilley's equation for the pressure perturbation.

Phillip's Equation

- Assume locally parallel mean flow and take divergence of Eqn. 2, applying the relation of Eqn. 3, we obtain Phillip's equation:

$$\frac{D^2 p}{Dt^2} - \frac{\partial}{\partial x_i}\frac{\gamma \bar{p}}{\bar{\rho}}\frac{\partial p}{\partial x_i} = 2\gamma \bar{p}\frac{\partial \bar{u}_j}{\partial x_i}\frac{\partial u_i}{\partial x_j} + \frac{\partial}{\partial x_i}\frac{\gamma \bar{p}}{\bar{\rho}}\frac{\partial q_s}{\partial x_i}. \tag{4}$$

- Performing the material derivative upon Eqn. 4, Lilley's equation is obtained:

$$\frac{D}{Dt}\left(\frac{D^2 p}{Dt^2} - \frac{\partial}{\partial x_i}\bar{c}^2\frac{\partial p}{\partial x_i}\right) + 2\frac{\partial \bar{u}_j}{\partial x_i}\frac{\partial}{\partial x_j}\bar{c}^2\frac{\partial p}{\partial x_i} = -2\bar{\rho}\bar{c}^2\frac{\partial \bar{u}_j}{\partial x_i}\frac{\partial \bar{u}_k}{\partial x_j}\frac{\partial u_i}{\partial x_k} + \frac{D}{Dt}\frac{\partial}{\partial x_i}\bar{c}^2\frac{\partial q_s}{\partial x_i}. \tag{5}$$

Lilley's Equation

- The first term on the right-hand side is zero for a locally parallel mean flow. Thus the equation governing the acoustic pressure in the medium is,

$$\frac{D}{Dt}\left(\frac{D^2p}{Dt^2} - \frac{\partial}{\partial x_i}\bar{c}^2\frac{\partial p}{\partial x_i}\right) + 2\frac{\partial \bar{u}_j}{\partial x_i}\frac{\partial}{\partial x_j}\bar{c}^2\frac{\partial p}{\partial x_i} = \Lambda. \tag{6}$$

- On the left-hand side is Lilley's operator.
- On the right-hand side is an equivalent source term:

$$\Lambda = \frac{D}{Dt}\frac{\partial}{\partial x_i}\bar{c}^2\frac{\partial q_s}{\partial x_i}. \tag{7}$$

Solution

- The solution of Eqn. 6 is the convolution of Green's function and source,

$$p(\mathbf{x},t) = \int_{-\infty}^{\infty} \dots \int_{-\infty}^{\infty} g(\mathbf{x},t|\mathbf{x}_s,t_s)\Lambda(\mathbf{x}_s,t_s)d\mathbf{x}_s dt_s. \tag{8}$$

- The integral can be rearranged by application of Green's second identity and integration by parts

$$p(\mathbf{x},t) = \int_{-\infty}^{\infty} \dots \int_{-\infty}^{\infty} \frac{Dq_s}{Dt_s}\nabla_s \cdot \bar{c}_s^2 \nabla_s g \; + \left[\frac{\partial g}{\partial x_s}\frac{1}{r_s}\frac{\partial}{\partial r_s}\left(r\bar{c}_s^2\frac{\partial \overline{u}_s}{\partial r_s}\right) - \frac{\partial}{\partial r_s}\left(\bar{c}_s^2\frac{\partial \overline{u}_s}{\partial r_s}\frac{\partial g}{\partial x_s}\right)\right] q_s d\mathbf{x}_s dt_s. \tag{9}$$

Acoustic Pressure

- Representing g by its inverse Fourier transform, the pressure solution becomes:

$$p(\mathbf{x},t) = \int_{-\infty}^{\infty} \dots \int_{-\infty}^{\infty} \mathcal{G}(\mathbf{x},\mathbf{x}_s,\omega)\frac{Dq}{Dt}(\mathbf{x}_s,t_s)e^{-i\omega(t-t_s)}d\omega d\mathbf{x}_s dt_s + \int_{-\infty}^{\infty} \dots \int_{-\infty}^{\infty} \mathbb{G}(\mathbf{x},\mathbf{x}_s,\omega)q(\mathbf{x}_s,t_s)e^{-i\omega(t-t_s)}d\omega d\mathbf{x}_s dt_s. \quad (10)$$

and

$$\mathcal{G} = \nabla_s \cdot \overline{c}_s^2 \nabla_s G$$

$$\mathbb{G} = \left[\frac{\partial G}{\partial x_s}\frac{1}{r_s}\frac{\partial}{\partial r_s}\left(r\overline{c}_s^2\frac{\partial \overline{u}_s}{\partial r_s}\right) - \frac{\partial}{\partial r_s}\left(\overline{c}_s^2\frac{\partial \overline{u}_s}{\partial r_s}\frac{\partial G}{\partial x_s}\right)\right]$$

Source Correlation

- Wiener-Khintchine theorem:

$$S(\mathbf{x},\omega) = \frac{1}{2\pi}\int_{-\infty}^{\infty} \langle p(\mathbf{x},t), p(\mathbf{x},t+\tau)\rangle e^{i\omega\tau} d\tau. \tag{11}$$

- Models of the source correlations are required for the pressure autocorrelation.
- Model for the source statistics matches Tam and Auriault [6].
- Model matches measurements of Davies et al. [9] and can be simply integrated.

$$\left\langle \frac{Dq}{Dt}(\mathbf{x}_1,t_1), \frac{Dq}{Dt}(\mathbf{x}_2,t_2)\right\rangle = \frac{\hat{q}_s^2}{\tau_s^2}\exp\left[-\frac{|\xi|}{\bar{u}\tau_s} - \frac{ln(2)}{l_s^2}\left((\xi-\bar{u}\tau)^2+\eta^2+\zeta^2\right)\right] \tag{12}$$

$$\left\langle q(\mathbf{x}_1,t_1), q(\mathbf{x}_2,t_2)\right\rangle = \hat{q}_s^2\exp\left[-\frac{|\xi|}{\bar{u}\tau_s} - \frac{ln(2)}{l_s^2}\left((\xi-\bar{u}\tau)^2+\eta^2+\zeta^2\right)\right] \tag{13}$$

Green's Function Relation

- Integration of Eqn. 11 can be performed over frequency and time to obtain

$$S(\mathbf{x},\omega) = \left(\frac{4\pi^3}{ln(2)}\right)^{\frac{1}{2}} \int_{-\infty}^{\infty} \cdots \int_{-\infty}^{\infty} \left[\mathcal{G}(\mathbf{x},\mathbf{x}_1,\omega_1)\mathcal{G}^*(\mathbf{x},\mathbf{x}_2,\omega_2)\frac{\hat{q}_s^2}{\tau_s^2} + \mathbb{G}(\mathbf{x},\mathbf{x}_1,\omega_1)\mathbb{G}^*(\mathbf{x},\mathbf{x}_2,\omega_2)\hat{q}_s^2\right] \times \frac{l_s}{\bar{u}} \exp\left[-\frac{|\xi|}{\bar{u}\tau_s} - \frac{ln(2)}{l_s^2}\left(\eta^2+\zeta^2\right)\right] \exp\left[-i\frac{\xi}{\bar{u}}\omega - \frac{l_s^2}{4\bar{u}^2 ln(2)}\omega^2\right] d\mathbf{x}_1\, d\mathbf{x}_2. \quad (14)$$

- The Green's functions at two source points can be related by a phase factor

$$\mathcal{G}^*(\mathbf{x},\mathbf{x}_1,\omega) \simeq \mathcal{G}^*(\mathbf{x},\mathbf{x}_2,\omega) \exp\left[\frac{i\omega}{c_\infty \|\mathbf{x}\|}\mathbf{x}\cdot\boldsymbol{\eta}\right], \quad (15)$$

$$\mathbb{G}^*(\mathbf{x},\mathbf{x}_1,\omega) \simeq \mathbb{G}^*(\mathbf{x},\mathbf{x}_2,\omega) \exp\left[\frac{i\omega}{c_\infty \|\mathbf{x}\|}\mathbf{x}\cdot\boldsymbol{\eta}\right]. \quad (16)$$

Spectral Density

- Integral of Eqn. 14 performed over $\mathbf{x}_1$

$$S(\mathbf{x},\omega) = 4\pi\left(\frac{\pi}{ln(2)}\right)^{3/2}\int_{-\infty}^{\infty}\int_{-\infty}^{\infty}\int_{-\infty}^{\infty}\hat{q}_s^2 l_s^3\left[\frac{1}{\tau_s}|\mathcal{G}(\mathbf{x},\mathbf{x}_s,\omega)|^2+\tau_s|\mathbb{G}(\mathbf{x},\mathbf{x}_s,\omega)|^2\right]$$
$$\times\exp\left[-\omega^2\frac{l_s^2}{4\bar{u}^2 ln(2)}\right]\Big/\left[1+\omega^2\tau_s^2\left(1-\frac{\bar{u}}{c_\infty}cos\theta\right)^2\right]d\mathbf{x}_s. \quad (17)$$

- For the cases considered: $\frac{1}{\tau_s}|\mathcal{G}(\mathbf{x},\mathbf{x}_s,\omega)|^2 >> \tau_s|\mathbb{G}(\mathbf{x},\mathbf{x}_s,\omega)|^2$
- Final spectral density integral:

$$S(\mathbf{x},\omega) = 4\pi\left(\frac{\pi}{ln(2)}\right)^{3/2}\int_{-\infty}^{\infty}\int_{-\infty}^{\infty}\int_{-\infty}^{\infty}\frac{\hat{q}_s^2 l_s^3}{\tau_s}|\mathcal{G}(\mathbf{x},\mathbf{x}_s,\omega)|^2$$
$$\times\exp\left[-\omega^2\frac{l_s^2}{4\bar{u}^2 ln(2)}\right]\Big/\left[1+\omega^2\tau_s^2\left(1-\frac{\bar{u}}{c_\infty}cos\theta\right)^2\right]d\mathbf{x}_s. \quad (18)$$

Comparison to Tam Model

Component	**Tam Model**	**Current Model**
Governing Equation	Linearized Euler Eqns. (LEE)	Lilley's Eqn.
Source Model	$q_s = \frac{2}{3}\rho k_s$	$q_s = \frac{2}{3}\rho k_s$
Source Correlation	Tam Correlation	Tam Correlation
Turbulence Model	Thies and Tam $k-\epsilon$ [10]	Mentor $k-\omega$ [11]
Green's Function	Adjoint solution to LEE	Modified Lilley $\mathcal{G} = \nabla \cdot \bar{c}^2 \nabla G$

Free Space Green's Function

- When neglecting mean flow refraction effects, G_0 is the solution to the Helmholtz equation,

$$\frac{\omega^2}{c_\infty^2} G_0 + \frac{\partial^2 G_0}{\partial x_i \partial x_i} = \frac{-i}{2\pi\omega c_\infty^2} \delta(\mathbf{x} - \mathbf{x}_s). \tag{19}$$

- The solution to G_0 is well known. Computing $\nabla \cdot \bar{c}^2 \nabla G_0$ we get,

$$\mathcal{G}_0(\mathbf{x}, \mathbf{x}_s, \omega) = \frac{-i\omega}{8\pi^2 c_\infty^2} \frac{\exp\left(i\frac{\omega}{c_\infty} R\right)}{R} = \frac{-i\omega}{2\pi c_\infty^2} G_f. \tag{20}$$

Refraction Effects

- To incorporate mean flow refraction effects, use a high-frequency asymptotic Green's function obtained by Balsa [12] and Wundrow and Khavaran [13],

$$G_q\left(\boldsymbol{x}, \boldsymbol{x}_s, \omega\right) \sim \frac{-i}{\overline{c}_s c_\infty \omega} \frac{1}{\left(1 - M_s cos\theta\right)^2} G_f \mathcal{R}_\omega, \tag{21}$$

- $\mathcal{R}_\omega$ is found using WKB approach,

$$\mathcal{R}_\omega \sim \exp\left[i \frac{\omega}{c_\infty}\left(\chi - R\sin^2\left(\theta\right) - \chi_s \cos\left(\phi - \phi_s\right)\right)\right]. \tag{22}$$

- χ is a function of the mean flow such that

$$\chi(r) = \int_0^r \mathcal{Q}(r')dr',$$
$$\mathcal{Q} = \sqrt{\Phi^2 - \cos^2(\theta)},$$
$$\Phi(r) = \frac{c_\infty - \overline{u}\cos(\theta)}{\overline{c}}.$$

Refraction Effects

- Balsa Green's function is obtained with the assumption that the source is close to the centerline axis.
- When deriving $\mathcal{G}_q = \nabla_s \cdot \bar{c}_s^2 \nabla_s G_q$, we must consider that
  - Terms that scale as r_s^{-1} or r_s^{-2} will dominate.
  - The acoustic field is nearly axisymmetric, $\partial/\partial\phi = 0$.
  - Neglect terms of $O(R^{-2})$ or smaller.

$$\mathcal{G}_q = \frac{\bar{c}_s^2 G_q}{r_s}\left(-\frac{\bar{c}_s'}{\bar{c}_s} + \frac{2M_s' \cos\theta}{1 - M_s\cos\theta} - \frac{ik_0}{4\pi}\frac{r\cos(\phi-\phi_s)}{R}\right) + \frac{ik_0\bar{c}_s^2 G_q}{r_s}\left(\cos(\phi-\phi_s)\frac{r^3}{R^3} - \frac{2r}{R} - Q_s\cos(\phi-\phi_s)\right). \quad (23)$$

Shielding Effects

- Ffowcs-Williams and Hall obtained a solution to the Helmholtz Green's function with a semi-infinite plate in the far-field,

$$G_t\left(\boldsymbol{x};\boldsymbol{x}_s,x_p,y_p,\omega\right)=\frac{e^{(1/4)\kappa\pi}}{\sqrt{\pi}}\frac{e^{-i\kappa R}}{4\pi R}\int_{-\infty}^{u_R}e^{-iu^2}du + \frac{e^{(1/4)\kappa\pi}}{\sqrt{\pi}}\frac{e^{-i\kappa R'}}{4\pi R'}\int_{-\infty}^{u_{R'}}e^{-iu^2}du. \quad (24)$$

- Acoustic waves in the far-field are governed by the Helmholtz equation.
- Thus, we propose to replace G_f in Eqns. 20 and 23 with G_t.

RANS

- Turbulence scales l_s and τ_s and source term q_s obtained from RANS.
- $k - \omega$ turbulence model
- RANS simulation validated with the PIV data of Bridges and Wernet [14] for NPR = 1.861 and TTR = 1.00.

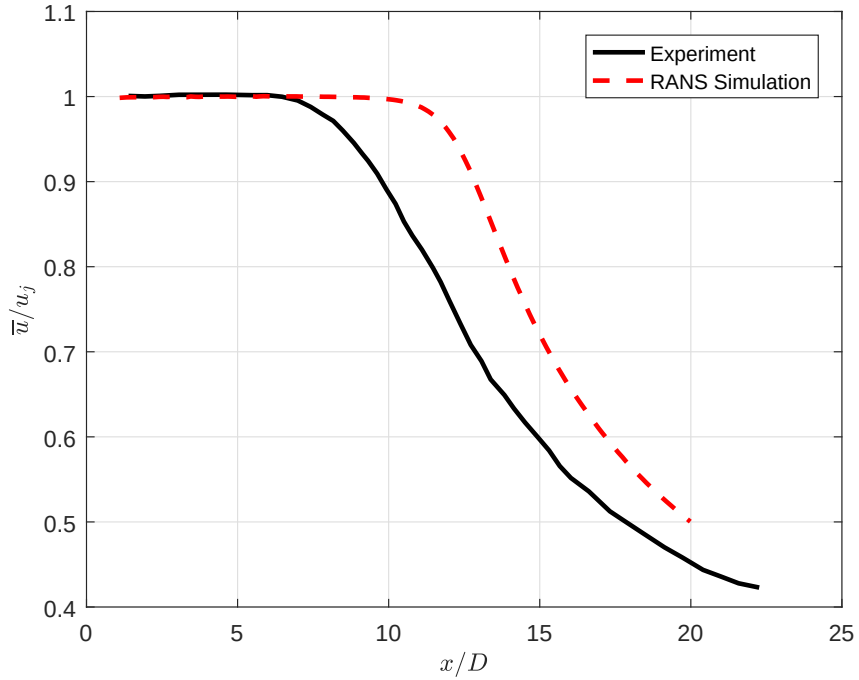

Figure 1: RANS centerline velocity profile compared to the PIV data of Bridges and Wernet [14] for NPR = 1.861 and TTR = 1.00

RANS

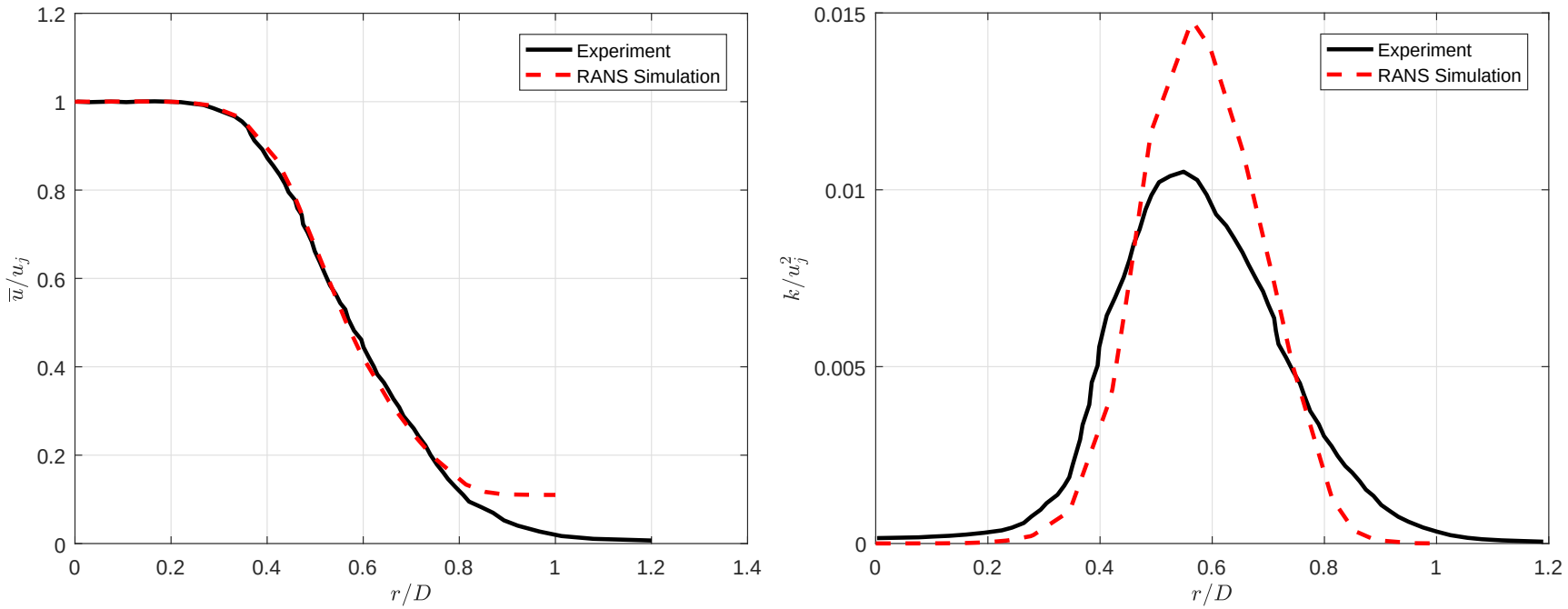

(a) u (b) TKE

Figure 2: RANS velocity and turbulent kinetic energy profile at $xD^{-1} = 4$ compared to the PIV data of Bridges and Wernet [14] for NPR = 1.861 and TTR = 1.00.

Setpoints

- Scaling coefficient c_q and turbulence coefficients c_τ, and c_l are calibrated for an observer angle of $\theta = 90°$ with $M_j = 0.985$ and TTR $= 1.00$.
- Predictions are compared to three subsonic setpoints of Brown and Bridges [1].

Table 1: Experimental Setpoints of Brown and Bridges [1].

Setpoint	M_j	TTR	NPR
3	0.513	1.00	1.197
5	0.725	1.00	1.418
7	0.985	1.00	1.861

Mach Number Scaling

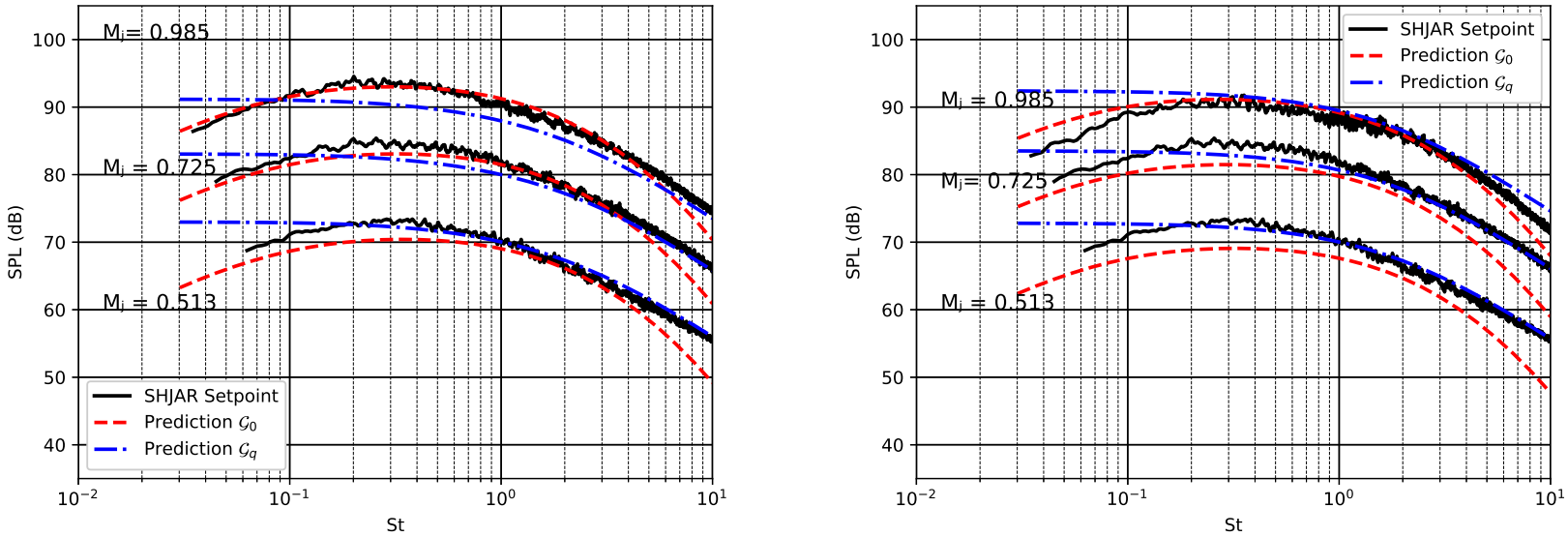

(a) $\theta = 90°$ (b) $\theta = 120°$

Figure 3: Comparison of SPL at $R = 100D$ and $\phi = 0°$, for a) $\theta = 90°$ and b) $120°$. Setpoints 3, 5, and 7 are considered, corresponding to $M_j = 0.513$, $M_j = 0.725$, and $M_j = 0.985$, respectively. Experimental measurements are from Brown and Bridges [1].

Freejet Predictions

- Predictions are compared across a range of observer angles, 70-130°.
- Validity of G_q is restricted to these angles.

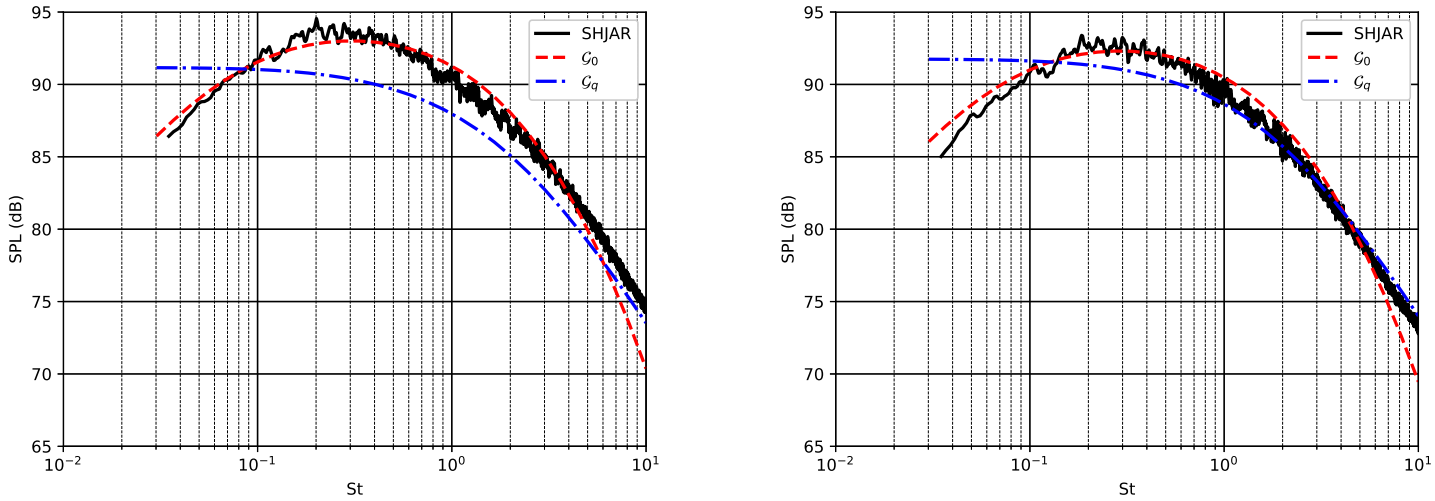

(a) $\theta = 90°$ (b) $\theta = 100°$

Figure 4: Comparison of SPL at $R = 100D$, $90° \leq \theta \leq 120°$, and $\phi = 0°$. Jet operating at setpoint 7, compared to Brown and Bridges [1].

Freejet Predictions

- Better agreement between $\mathcal{G}_q$ and experimental measurements at large Strouhal number.

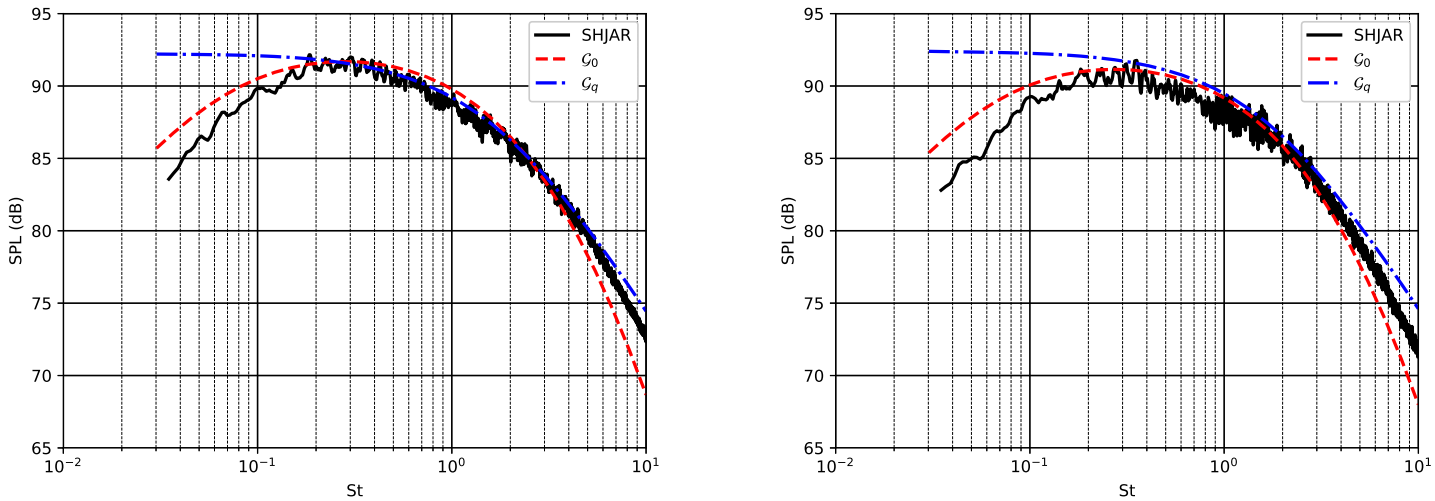

(a) $\theta = 110°$ (b) $\theta = 120°$

Figure 5: Comparison of SPL at $R = 100D$, $90° \leq \theta \leq 120°$, and $\phi = 0°$. Jet operating at setpoint 7, compared to Brown and Bridges [1].

Semi-Infinite Flat Plate

- Consider a semi-infinite plate present in the far-field.
- Acoustic spectrum will decrease significantly for observer angles that are shielded by the plate.
- Will replacing G_f by G_t effectively capture the drop in SPL?
- Start by comparing predictions with measurements for a flat plate at $xD^{-1} = 15$ and $rD^{-1} = 16$ for jet at setpoint 7.
- Then compare over a wider range of observer angles for two values of Strouhal number (St $= 3$, and 4).

Prediction of SPL Drop

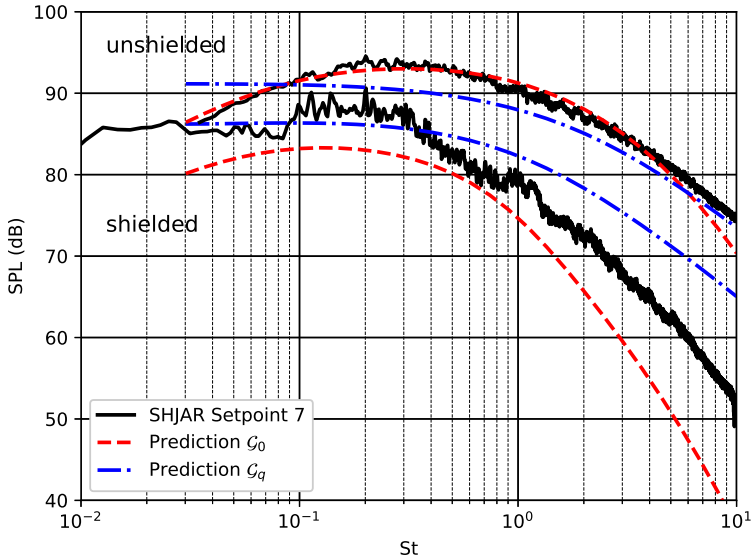

(a) $\theta = 90°$

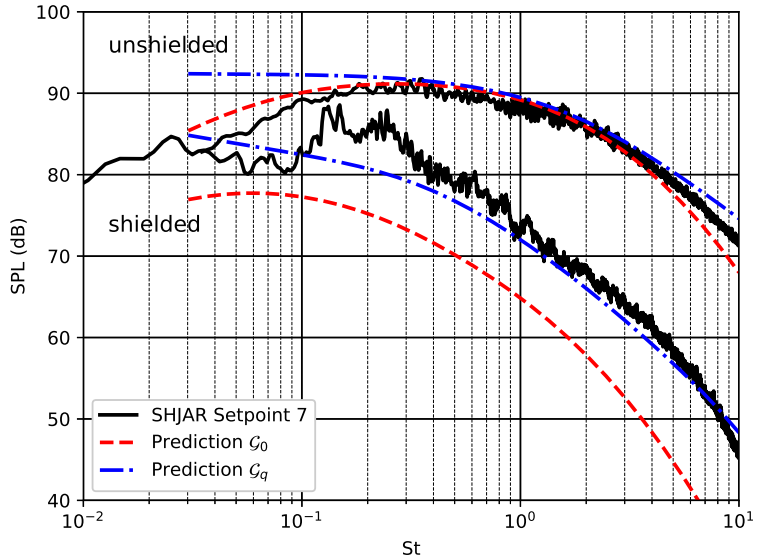

(b) $\theta = 120°$

Figure 6: Comparison of SPL on the shielded side of a flat plate ($xD^{-1} = 15$ and $rD^{-1} = 16$) at $R = 100D$, $\theta = 90°$ and $120°$, and $\phi = 0°$ from the nozzle center. The jet is issuing from a SMC000 convergent nozzle operating at $M = 0.985$, NPR = 1.861, and TTR = 1.00. Experimental measurements obtained from Brown [2].

Range of Observer Angles

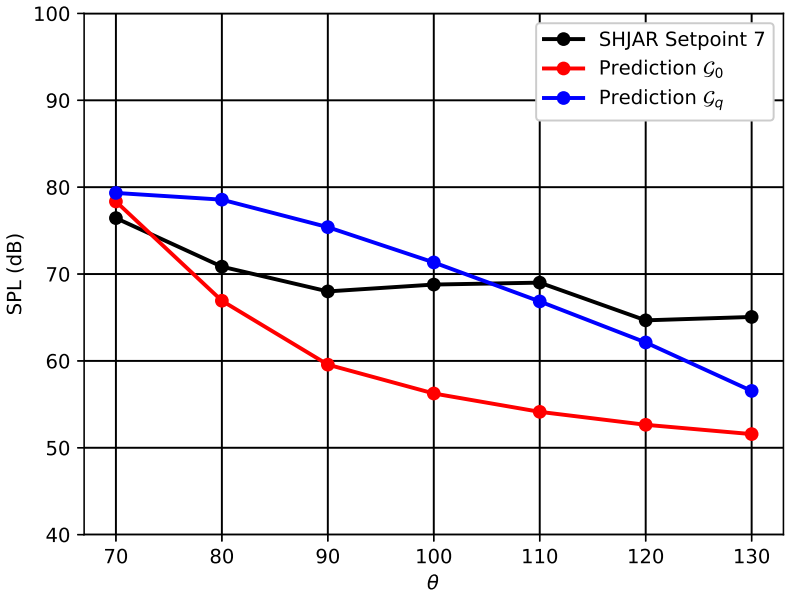

(a) $St = 3$

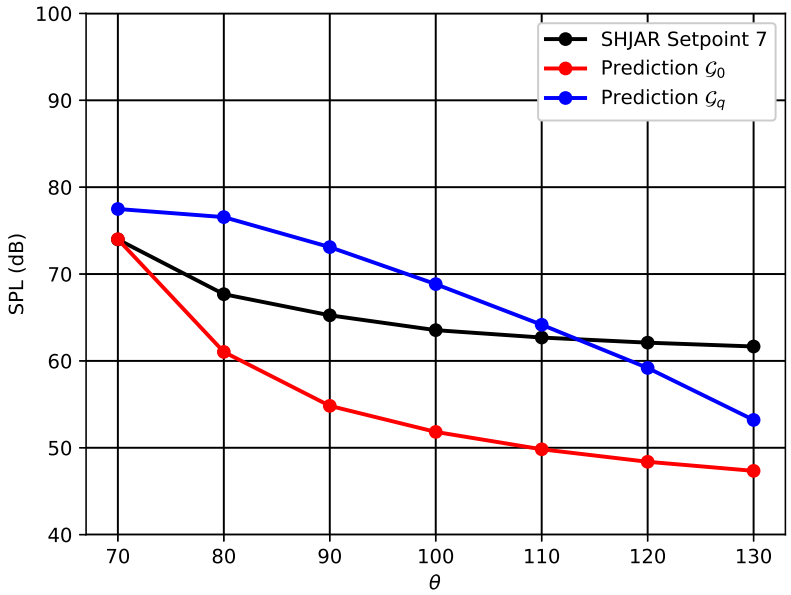

(b) $St = 4$

Figure 7: Comparison of SPL on the shielded side of a flat plate ($xD^{-1} = 15$ and $rD^{-1} = 16$) at $R = 100D$ and $\phi = 0°$ from the nozzle center. Predictions are computed at several different observer angles $70° \leq \theta \leq 130°$ from the downstream axis for 4 different Strouhal numbers. The jet is issuing from a SMC000 convergent nozzle operating at $M = 0.985$, NPR = 1.861, and TTR = 1.00. Experimental measurements obtained from Brown [2].

Summary

- Fine-scale noise prediction formulated in terms of Lilley's equation.
- Spectral density integral differs from Tam and Auriault [6] only by the Green's function.
- Favorable predictions obtained for unheated subsonic freejets at high Strouhal number
- Refraction effects modeled with analytical Green's function.
- Shielding predictions show slight improvement in SPL magnitude. However, do not capture relationship between SPL and θ.

Thank You

Questions?

References I

[1] C. Brown and J. Bridges, "Small hot jet acoustic rig validation," Tech. Rep. 20060013451, NASA Glenn Research Center, apr 2006.

[2] C. Brown, "Jet-surface interaction test: Far-field noise results," in *Volume 1: Aircraft Engine, Ceramics, Coal, Biomass and Alternative Fuels, Controls, Diagnostics and Instrumentation*, ASME, June 2012.

[3] A. Khavaran, E. A. Krejsa, and C. M. Kim, "Computation of supersonic jet mixing noise for an axisymmetric convergent-divergent nozzle," *Journal of Aircraft*, vol. 31, no. 3, pp. 603–609, 1994.

[4] Y. Khalighi, F. Ham, J. Nichols, S. Lele, and P. Moin, "Unstructured large eddy simulation for prediction of noise issued from turbulent jets in various configurations," in *17th AIAA/CEAS Aeroacoustics Conference (32nd AIAA Aeroacoustics Conference)*, American Institute of Aeronautics and Astronautics, AIAA 2011-2886, June 2011.

[5] J. E. Ffowcs Williams and D. L. Hawkings, "Sound generation by turbulence and surfaces in arbitrary motion," *Philosophical Transactions of the Royal Society A: Mathematical, Physical and Engineering Sciences*, vol. 264, pp. 321–342, May 1969.

[6] C. K. W. Tam and L. Auriault, "Jet mixing noise from fine-scale turbulence," *AIAA Journal*, vol. 37, pp. 145–153, 2 1999.

[7] P. J. Morris and F. Farassat, "Acoustic analogy and alternative theories for jet noise prediction," *AIAA Journal*, vol. 40, no. 4, pp. 671–680, 2002.

[8] J. Boussinesq, "Théorie des ondes et des remous qui se propagent le long d'un canal rectangulaire horizontal, en communiquant au liquide contenu dans ce canal des vitesses sensiblement pareilles de la surface au fond.," *Journal de Mathématiques Pures et Appliquées*, pp. 55–108, 1872.

[9] P. O. A. L. Davies, M. J. Fisher, and M. J. Barratt, "The characteristics of the turbulence in the mixing region of a round jet," *Journal of Fluid Mechanics*, vol. 15, pp. 337–367, Mar. 1963.

[10] A. T. Thies and C. K. W. Tam, "Computation of turbulent axisymmetric and nonaxisymmetric jet flows using the k-epsilon model," *AIAA Journal*, vol. 34, no. 2, pp. 309–316, 1996.

References II

[11] F. R. Mentor, "Improved two-equation k-ω turbulence models for aerodynamic flows," Technical Report NASA-TM-103975, A-92183, NAS 1.15:103975, NASA Ames Research Center, Oct 1992.

[12] T. F. Balsa, "The far field of high frequency convected singularities in sheared flows, with an application to jet-noise prediction," *Journal of Fluid Mechanics*, vol. 74, pp. 193–208, Mar. 1976.

[13] D. W. Wundrow and A. Khavaran, "On the applicability of high-frequency approximations to lilley's equation," *Journal of Sound and Vibration*, vol. 272, pp. 793–830, May 2004.

[14] J. Bridges and M. P. Wernet, "The nasa subsonic particle image velocimetry (piv) dataset," Technical Report NASA/TM-2011-216807, NASA Glenn Research Center, Nov 2011.

Extra Slides

Source Location

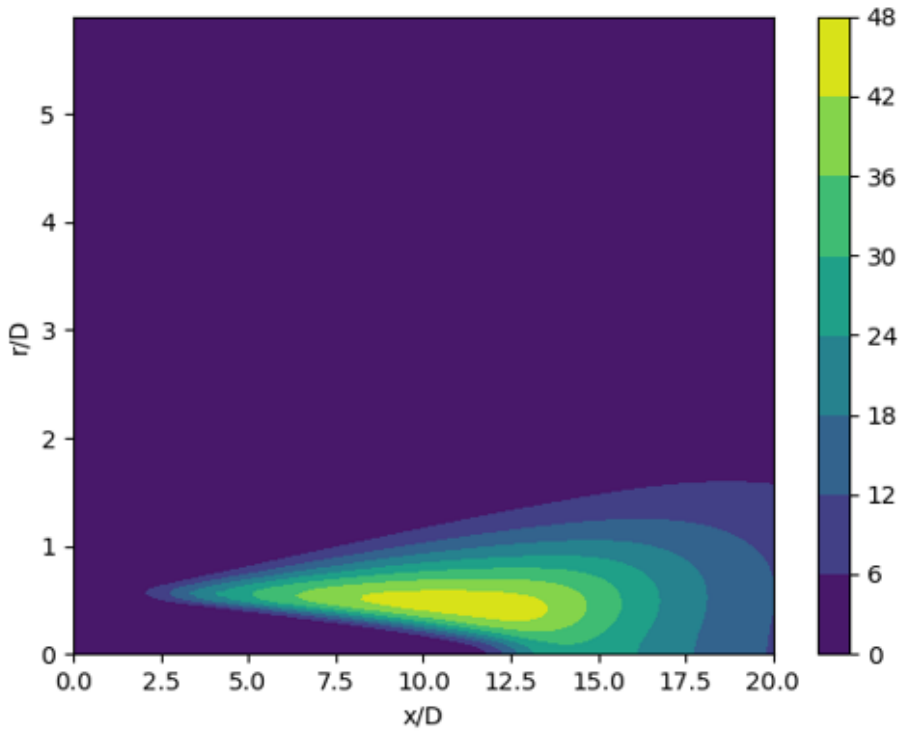

Figure 8: Contour plot of source magnitude obtained from the steady RANS $k-\omega$ Menter SST model. Jet is operating at M=0.985 and TTR = 1.0.

High Frequency Green's function Validation

- Prescribed mean flow profile of Wundrow and Khavaran [13] for $M_j = 0.9$

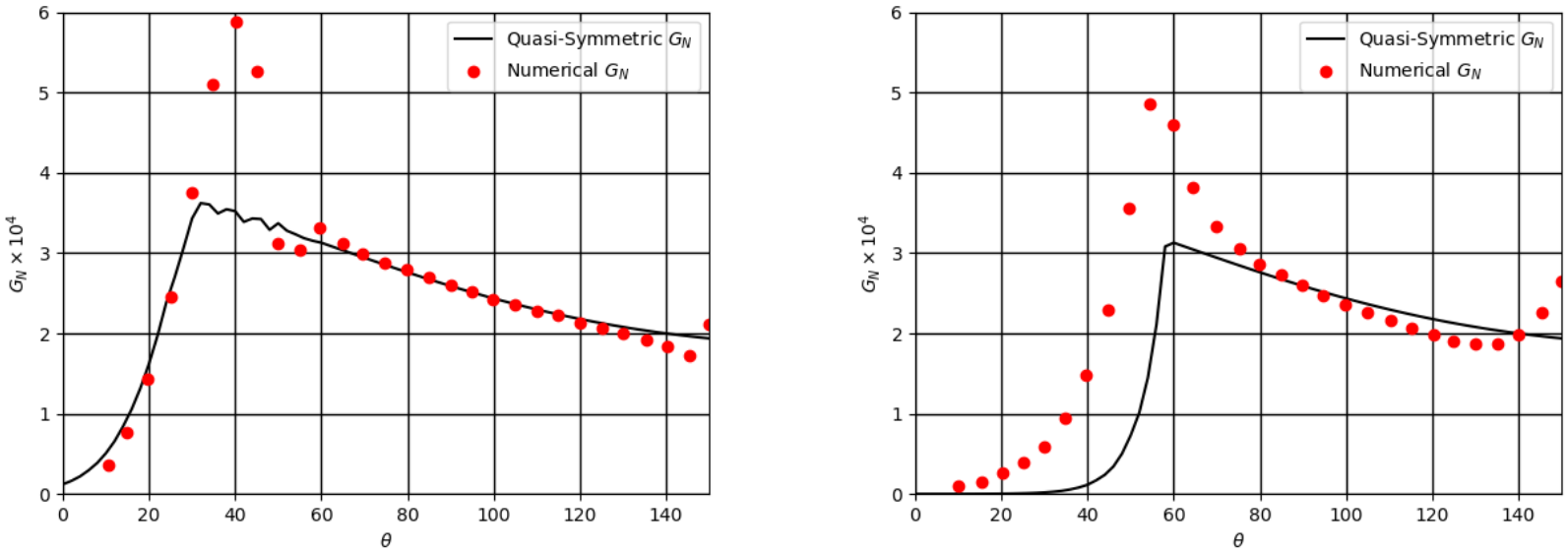

(a) $\phi = 0°$ (b) $\phi = 90°$

Figure 9: Normalized magnitude of G_q for a prescribed mean flow

Solution Integral Rearrangement

- Λ can be re-arranged to the following form in a cylindrical coordinate system,

$$\frac{D}{Dt}\nabla\cdot\overline{c}^2\nabla q_s = \nabla\cdot\overline{c}^2\nabla\frac{Dq_s}{Dt} - \left[\frac{1}{r}\frac{\partial}{\partial r}\left(r\overline{c}^2\frac{\partial\overline{u}}{\partial r}\frac{\partial q_s}{\partial x}\right) + \overline{c}^2\frac{\partial\overline{u}}{\partial r}\frac{\partial^2 q_s}{\partial r\partial x}\right]. \tag{25}$$

- The convolution integral of the first term in Eqn. 25 with the Green's function can be rearrange by making use of Green's second identity,

$$\int_{-\infty}^{\infty}\int_{-\infty}^{\infty}\int_{-\infty}^{\infty} g(\mathbf{x},t|\mathbf{x}_s,t_s)\nabla\cdot\overline{c}^2\nabla\frac{Dq_s}{Dt}d\mathbf{x} = \oiint_S \overline{c}^2\left(g\frac{\partial}{\partial\mathbf{n}}\left(\frac{Dq_s}{Dt}\right) - \frac{Dq_s}{Dt}\frac{\partial g}{\partial\mathbf{n}}\right)dS + \int_{-\infty}^{\infty}\int_{-\infty}^{\infty}\int_{-\infty}^{\infty}\nabla\cdot\overline{c}^2\nabla g\frac{Dq_s}{Dt}d\mathbf{x}. \tag{26}$$

Solution Integral Rearrangement

- The surface integral can be evaluated beyond the jet boundary, where $q = 0$, and thus becomes negligible.
- The convolution integral of g with the remaining term of Eqn. 25 can be rearranged using integration by parts.

$$p(\mathbf{x},t) = \int_{-\infty}^{\infty} \cdots \int_{-\infty}^{\infty} \frac{Dq_s}{Dt_s} \nabla_s \cdot \bar{c}_s^2 \nabla_s g + \left[\frac{\partial g}{\partial x_s} \frac{1}{r_s} \frac{\partial}{\partial r_s} \left(r \bar{c}_s^2 \frac{\partial \overline{u}_s}{\partial r_s} \right) - \frac{\partial}{\partial r_s} \left(\bar{c}_s^2 \frac{\partial \overline{u}_s}{\partial r_s} \frac{\partial g}{\partial x_s} \right) \right] q_s d\mathbf{x}_s dt_s. \quad (27)$$